Detailed Design of a High Speed Switched Reluctance Starter/Generator for More/All Electric Aircraft

Song Shoujun[a,b,*], Liu Weiguo[a], Dieter Peitsch[c], Uwe Schaefer[b]

[a]*School of Automation, Northwestern Polytechnical University, Xi'an 710072, China*

[b]*School of Electrical Engineering and Computer Sciences, Technical University of Berlin, Berlin 10587, Germany*

[c]*School of Mechanical Engineering and Transport Systems, Technical University of Berlin, Berlin 10587, Germany*

Abstract

The basic concepts and advantages of more/all electric aircraft (M/AEA) are briefly addressed. The combined starter/generator (CS/G) system is introduced as a key technology to enable M/AEA. Some important performance requirements for CS/G system are obtained. Based on these requirements, a high speed switched reluctance machine (SRM) is designed to operate as a starter/generator. The entire design process is mainly divided into two stages: electromagnetic design and thermal design. In electromagnetic design stage, the electromagnetic structure and dimensions of the machine and the number of phase winding turns per pole are obtained; the topology and main technical details of the converter are briefly introduced as well. In thermal design stage, a liquid-cooling system is designed based on the thermal analysis of the machine. In the end, the performances of the designed SRM are basically verified by simulation. To get high performances, the exciting angles are optimized in two different operating modes respectively, and the optimized performances in the motoring mode are given as well.

Keywords: aircraft; more/all electric aircraft; combined starter/generator system; reluctance motors; electromagnetic design; thermal analysis; control; optimization

Nomenclature

List of principal symbols:

T	Output torque, N·m
r_r, D_r	Rotor radius and diameter, m
L_{stk}	Stack length, m
r_s, D_s	Stator radius and diameter, m
L_e	Overall length, m
g	Airgap length, m
β_r, β_s	Rotor and stator pole arcs, (°)
m	Number of phases
N_r	Number of rotor poles
r_{sh}, D_{sh}	Shaft radius and diameter, m
N_p	Number of turns per pole
ψ	Flux-linkage, Wb
ω	Angular velocity of the rotor, rad/s
$\theta_{on}, \theta_{off}$	Turn-on and turn-off angles, rad
V_s	DC supply voltage, V
R	Resistance of the phase winding, Ω
i	Phase current, A
θ	Rotor angular position, rad
ψ_{peak}	Peak flux-linkage, Wb
Δ	Conduction dwell angle, rad
ω_n	Specified speed, rad/s
B_s	Saturation flux density, T
I_{rms}	Rms phase current, A
C_h	Hysteresis loss coefficient
f	Electrical frequency, Hz
B_{max}	Maximum magnetic flux density, T
C_e	Eddy-current loss coefficient
ρ_{air}	Density of the air, kg/m^3
μ_a	Dynamic viscosity of the air, kg/(s·m)
k_{cy}	Cylinder thermal conductivity, W/(m·K)
k_{ir}	Thermal conductivity of iron, W/(m·K)
R_{sc}	Surface cooling thermal resistance, K/W
h_{sc}	Heat transfer coefficient of surface cooling, W/(m^2·K)
A_{os}	Area of stator outer surface including cooling system, m^2
r_{s1}	Stator outer radius including cooling system, m
R_{wc}	Water cooling thermal resistance, K/W
h_{wc}	Heat transfer coefficient of water cooling, W/(m^2·K)

---

*Corresponding author. Tel.: +86-29-88431309.
E-mail address: songshoujun@hotmail.com

A_{ws} Contact surface area between stator steel and water, m^2

r_{w1}, r_{w2} Water channel outer and inner radius, m

r_{w3} Water channel round end radius, m

Re_{D_h} Reynolds number

v Kinematic viscosity of the water, m^2/s

Nu_{D_h} Nusselt number

Pr Prandtl number

k_w Thermal conductivity of water, W/(m·K)

1. Introduction

The more/all electric aircraft (M/AEA) concept has been discussed for many years as the future trendsetter in the aerospace industry[1-5]. It is based on the utilization of electric power to drive aircraft subsystems historically powered by a combination of hydraulic, pneumatic, and mechanical means including utility and flight control actuation, environmental control system, lubrication and fuel pumps, and numerous other utilities. Many studies have indicated that this concept offers significant aircraft level benefits in terms of reliability, maintainability, survivability, much lower operating and supporting costs, less impact on the environment, and improved performance. The system level payoffs that can be realized with more electric aircraft (MEA) for both military and commercial aircraft applications were discussed in Ref.[2]. Ref.[3] presented a brief history of the MEA concept and the reasons that the authors believe in its bright future. In Refs.[4]-[5], the history of M/AEA, some key technologies used in it, and its benefits are covered.

Previous studies to date indicate that the combined starter/generator (CS/G) system is a key subsystem concept required to enable M/AEA[2]. In this application the starter/generator will be the source of primary aircraft electric power and will also provide engine starting. The advantages of this concept are numerous. In all electric aircraft, the CS/G system will be integrated into the propulsion engine's turbine core. Integrating the CS/G system into the engine will eliminate the engine tower shaft and gears, power take-off shaft, and accessory drive gearboxes along with the need for gear lubrication and associated cooling systems, which will significantly reduce aircraft frontal area and drag torque during engine starting. In Ref.[6], the potential candidacy of induction and reluctance machine variable speed constant frequency (VSCF) drive technologies for aircraft starter/generator systems was discussed. J. A. Weimer[7] summarized technology developments, including starter/generator systems, which enable the MEA.

There are many kinds of machines that can be used as CS/G. The switched reluctance starter/generator (SRS/G) system is considered as a prime candidate technology that meets the requirements and constraints of the aircraft applications. The salient features of the SRS/G system include the ability to operate under fault conditions, the suitability to operate in high speeds and harsh environment, and the power density to be comparable to any other conventional machines. In Refs.[8]-[10], the design, implementation and test validation of SRS/G system for aircraft engine application were presented.

In this article, some important performance requirements for CS/G system are obtained firstly based on the typical 30 s starting procedure of the aircraft engine. Based on these requirements, a high speed switched reluctance machine (SRM) is designed to operate as a CS/G. The design comprises two main stages: electromagnetic design and thermal design. In electromagnetic design stage, the detailed derivation of the SRM dimensions is given. What's more, the topology and main technical details of the converter are briefly introduced. In thermal design stage, the thermal analysis of the machine is carried out. The simplified thermal model of the SRM is built, and the temperature rise curve of the winding is given. Finally, a liquid-cooling system is designed. After finishing the design, the performance of the SRM is verified basically by simulation. The results indicate that the designed SRM satisfies the requirements without the need for any further optimization. At the end of this article, the optimal control strategies are briefly presented in motoring and generating modes respectively, and the optimized performances in motoring mode are given as an example.

2. Analysis of Starting Procedure[11]

Engine start is initiated by setting the throttle to the ground idle position and switching on the starter. Then the starting cycle goes automatically. Fig.1 shows the typical 30 s starting procedure in terms of engine speed, temperature and starter torque.

Fig.1 indicates that once the starter accelerates the engine to about 8% of the ground idle speed, ignition is switched on. Then the engine speed increases further, while airflow through the engine grows accordingly. After reaching the lowest possible air mass flow rate for ignition, fuel will be injected.
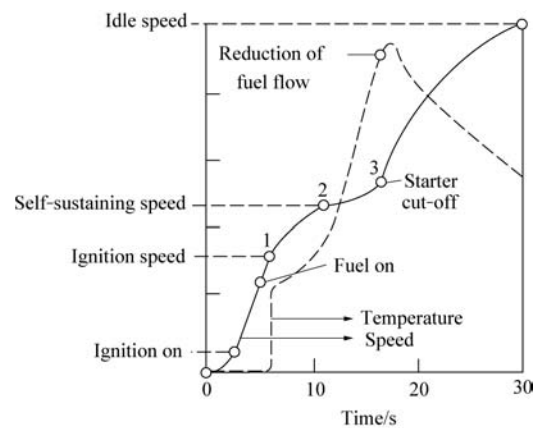
(a) Engine rotation speed and temperature
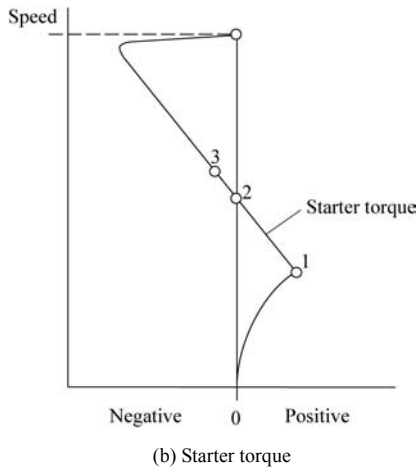
(b) Starter torque

Fig.1   Typical starting process of an aircraft engine.

The engine then begins to produce torque itself, but still requires support from the starter. When the engine reaches the self-sustaining speed, the starter motor curve crosses the zero-torque line, where the engine torque equals the starter torque. Only then is the engine power sufficient to accelerate the engine to idle speed. During this phase, the starter will be cut off and fuel flow will be adjusted to flight idle. This is the complete starting process of engine.

In general, it is beneficial if the starter motor continues to contribute to engine rotation long enough to cut down the starting duration, as engine and starter combined will reach ground idle speed much faster. In this article, the SRM will operate as a motor to accelerate the engine until the idle speed is reached.

According to the analysis of the engine starting process and the determination of some important performance parameters, Fig.2 shows the performance requirements for a CS/G system used in aircraft.
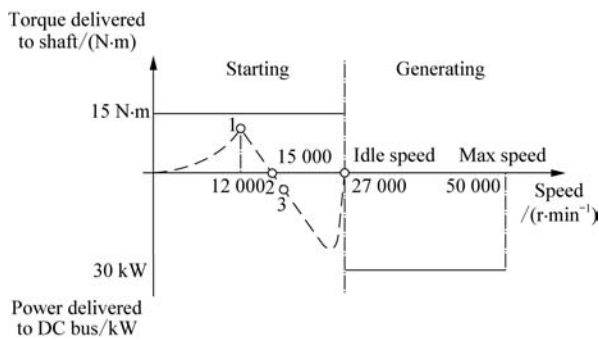

Fig.2   Performance requirements for CS/G system (The abscissa represents the shaft speed of the CS/G. It is three times as fast as that of the engine).

During the stage of engine start, the SRM operates as a motor and supplies torque to the engine from standstill to 2.7×10^4 r/min where the engine gets its idle speed of about 0.9×10^4 r/min. During this stage, the torque of the SRM must be bigger than 15 N·m (bigger than the torque needed at Point 1) to guarantee

the safe and quick start-up of the engine. Once the engine reaches its idle speed, the SRM becomes a generator to supply 270 V/30 kW DC electric power to the engine and other airborne electrical loads, and the maximum speed is 5.0×10^4 r/min. Based on the performance requirements indicated in Fig.2, the design process of SRM can be started.

3. Electromagnetic Design of SRM

The targets of electromagnetic design are to determine the geometric dimensions of the machine and the number of phase winding turns per pole according to the above-mentioned performance requirements. Additionally, the topology and ratings of the converter are briefly introduced.

3.1. Structure and dimensions of the machine[12]

There are several topologies of SRM differentiated by phase number and combinations of the stator and rotor poles. With higher phase-numbers, the torque ripple will be reduced, but it will increase the complexity of the motor structure, the number of the main switching devices and the cost of the whole system synchronously. However, if the number of the phases is less than three, the motor will lose its ability of self-starting. The advantage of the large pole-numbers is a smaller stroke angle, leading possibly to a lower torque ripple, but inevitably the price paid is a lower inductance ratio which may increase the controller volt-amperes and decrease the specific output. What's more, with higher pole-numbers, the core losses may be increased because of the higher switching frequency. In this article, 3-phase 6/4 topology is adopted, since noise will be negligible compared to the turbine.

After the determination of the numbers of phases and poles, the calculation of the dimensions can be started. There are two traditional methods which can be used, one is presented in Ref.[12], called Method 1, and the other one is described in Ref.[13], called Method 2. The calculation procedures of these two methods are similar; both of them are based on the output equation. The only difference is the input parameters. Method 1 uses the output equation in terms of the torque, while Method 2 uses power. Eq.(1) and Eq.(2) show these two types of output equations respectively. In Eq.(1), k is the output coefficient proportional to the product of the electric and magnetic loadings. For the definitions of the parameters in Eq.(2), refer to Ref.[13].

$$T = kD_r^2 L_{stk} \tag{1}$$

$$P_d = k_d k_1 k_2 A_{sp} B D_r^2 L_{stk} \eta N_r \tag{2}$$

It can be seen that designing with Method 2 should know the rated output power, efficiency and many other parameters in advance while with Method 1 only the output torque. According to the performance re-

quirements for the CS/G system under study (see Fig.2), Method 1 is adopted.

(1) Calculation of the envelope dimensions D_s and L_e

According to Eq.(1), to determine D_r and L_{stk} separately, it is necessary to select the length/diameter ratio L_{stk}/D_r, which typical value is 1, so Eq.(1) can be rewritten as

$$T = kD_r^3 \qquad (3)$$

In this article, k=30 kN/m² is adopted, it is a typical value for aerospace machines with liquid cooling. Together with the specified output torque 15 N·m, the rotor diameter can be obtained by Eq.(3) as D_r = 80 mm. Hence L_{stk} = 80 mm too.

The simplest way to estimate the stator diameter D_s is through the typical ratio of D_r/D_s which varies in a wide range of 0.40-0.70, and with most designs around 0.50-0.55. It depends on the number of stator and rotor poles and the operating requirements. The larger the number of poles, the larger this ratio tends to be. In this article, choosing D_r/D_s=0.50, so D_s=160 mm.

The overall length L_e is the sum of the stack length L_{stk} and twice the length of end-turn overhang,

$$L_e = L_{stk} + 2L_{oh} \qquad (4)$$

where the overhang length L_{oh} at each end can be estimated roughly as $1.2t_s$, t_s is the stator pole-width. Hence

$$L_e \approx L_{stk} + 2.4t_s \qquad (5)$$

The value of L_e can be easily obtained after the determination of t_s as follows.

(2) Calculation of other internal dimensions

The airgap length can be roughly estimated as 0.5% of the rotor diameter if the length/diameter ratio L_{stk}/D_r is 1. So, in this article, the airgap length $g = 0.005D_r$= 0.005×80 mm=0.4 mm.

There are some constraints on the selection of pole arcs β_s and β_r as follows:

$$\left. \begin{array}{l} \beta_r \geq \beta_s \\ \min(\beta_r, \beta_s) \geq \dfrac{2\pi}{mN_r} \\ \beta_r + \beta_s < 2\pi/N_r \end{array} \right\} \qquad (6)$$

In this article, β_s = 30° and β_r = 32° are selected.

The stator and rotor pole-width can be obtained through Eq.(7) and Eq.(8), respectively.

$$t_s = (D_r + 2g)\sin\frac{\beta_s}{2} \qquad (7)$$

$$t_r = D_r \sin\frac{\beta_r}{2} \qquad (8)$$

The results are t_s = 20.91 mm and t_r = 22.05 mm.

As the rotor yoke thickness y_r should be sufficient to carry the peak rotor flux without saturation, it should be at least equal to $t_r/2$, and preferably 20%-40% larger than $t_r/2$. In this article y_r = 0.65t_r ≈15 mm. The stator

yoke thickness y_s can be obtained by the similar method y_s = 0.65t_s ≈15 mm.

The slot depth of the rotor d_r should be at least 20-30 times the airgap length in order to obtain a low unaligned inductance. A useful guide is

$$d_r = t_s/2 \qquad (9)$$

then d_r = 10 mm.

The slot depth of the stator d_s needs to be as large as possible to maximize the winding area, making it easy to insert enough copper to minimize the copper losses. In this article, d_s can be obtained based on all the other dimensions determined above, giving

$$d_s = [D_s - D_r - 2(g + y_s)]/2 \qquad (10)$$

The result is d_s=24.6 mm.

The shaft diameter D_{sh} should be as large as possible to maximize the lateral stiffness of the rotor. This is of benefit to minimizing acoustic noise and to raising the first critical speed. In this article, D_{sh} can be determined by all the dimensions of the rotor mentioned above, giving

$$D_{sh} = D_r - 2(d_r + y_r) \qquad (11)$$

then D_{sh}=30 mm.

The cross-sectional view of the SRM with the dimensions calculated above is shown in Fig.3. All the dimensions are in millimeters. The materials of the lamination and the shaft are M270-35A and mild steel, respectively.

Fig.3   Cross-sectional view of machine without cooling system (all cylinders are dimensioned by their radius).

3.2. Number of turns per pole

In this article, it is assumed that there are N_p turns wound around each stator pole and the windings on opposite stator poles are connected in series to form a phase. As the value of N_p exerts significant influences

upon the performance of the system, its calculation is very important.

Based on the basic voltage equation of the phase winding, the flux linkage can be expressed by

$$\psi = \frac{1}{\omega} \int_{\theta_{\mathrm{on}}}^{\theta_{\mathrm{off}}} (V_{\mathrm{s}} - Ri)\mathrm{d}\theta \qquad (12)$$

The peak flux linkage can be estimated from Eq.(12) by assuming that at the specified speed there is no phase conduction overlap and winding/switching device voltage drops.

$$\psi_{\mathrm{peak}} = V_{\mathrm{s}}\Delta/\omega_{\mathrm{n}} \qquad (13)$$

Given $\omega_{\mathrm{n}} = 2.7\times10^4$ r/min = 2 827.43 rad/s, based on the assumption mentioned above, it can be obtained that

$$\Delta = \frac{2\pi}{mN_{\mathrm{r}}} \qquad (14)$$

Furthermore, the peak flux-linkage can also be defined in terms of the saturation flux density and machine dimensions as follows:

$$\psi_{\mathrm{peak}} = 2t_{\mathrm{s}}L_{\mathrm{stk}}B_{\mathrm{s}}N_{\mathrm{p}} \qquad (15)$$

By combining Eqs.(13)-(15), the following can be obtained

$$N_{\mathrm{p}} = \frac{\pi V_{\mathrm{s}}}{\omega_{\mathrm{n}}t_{\mathrm{s}}L_{\mathrm{stk}}B_{\mathrm{s}}mN_{\mathrm{r}}} \qquad (16)$$

In this article, B_{s} is selected as 1.7 T. From Eq.(16), the number of turns per pole of the designed SRM can be obtained as 9. Finally, it is adjusted to 11 on the basis of extensive simulations and detailed analysis.

In this article, the stator slot area of the designed SRM is 827.9 mm^2 and the slot fill factor is 0.4, finally, the diameter of the wire can be obtained as 4.38 mm by simple calculation.

According to Ref.[12], for aerospace machines with liquid cooling, the continuous current density should be limited to about 20 A/mm^2. In this article, in the motoring mode (short-term operation), the maximum current density is 12 A/mm^2, while in the generating mode (continuous operation), 8 A/mm^2 is adopted. The simulation results with optimal control mentioned in Section 5 verify that the current density of the windings in both operating modes would never exceed the maximum values.

3.3. Topology and ratings of the converter

The converter receives power from the 270 VDC power bus during engine starting and provides power to the 270 VDC bus during generating.

There are many kinds of topologies that can be used in SRS/G system. According to the comparison of converter semiconductor volt-ampere (VA) ratings and the special characteristics of the application, the asymmetric half-bridge circuit, shown in Fig.4, is adopted.
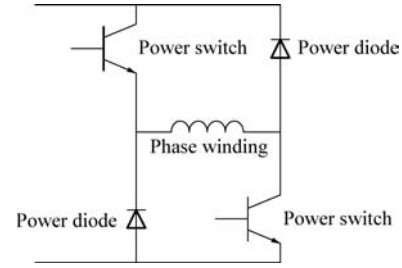
Fig.4   Converter topology (one phase of three).

It can be seen that the converter topology consists of two switches and two diodes per phase. The phase winding of the machine is in series with both switches, providing valuable protection against faults. The insulated gate bipolar transistors (IGBTs) with ratings of 600 V and 600 A are selected as power switches. The same ratings are with the power diodes. The maximum frequency stress of power devices is about 8 kHz and it occurs at half the rated speed.

4. Thermal Design of SRM

The target of thermal design is to build a suitable cooling system for the SRM through thermal analysis of the machine.

Since the temperature rise is caused by the power losses, in order to predict thermal behaviors of the machine, the power losses in the SRM must be calculated firstly.

4.1. Power losses in SRM

For the stator of the SRM, both the copper losses due to Joule effect and the iron losses due to hysteresis and eddy currents are considered while for the rotor, only iron losses occurs. In high speed electric machines, the air friction losses due to windage form a significant part of the total losses, so it is not negligible[14].

(1) Copper losses

The copper losses are caused by the current flowing through the windings, which can be easily got by

$$P_{\mathrm{cu}} = mI_{\mathrm{rms}}^2 R \qquad (17)$$

It should be noted that the influences of skin effect due to the high switching frequency can be avoided by employing stranded wires.

(2) Iron losses

The iron losses are proportional to the excitation magnetic motive force (MMF) and the stroke frequency. The approximate formula can be obtained based on Steinmetz equation as the sum of hysteresis and eddy-current losses:

$$P_{\mathrm{fe}} = C_{\mathrm{h}}fB_{\mathrm{max}}^n + C_{\mathrm{e}}f^2B_{\mathrm{max}}^2 \qquad (18)$$

In this article, C_{h}, C_{e} and exponent n have been calculated from measured data at 50 Hz and 400 Hz for M270-35A material[15].

Because of the presence of strong DC magnetization in SRM, Eq.(18) is a pessimistic approximation.

(3) Air friction losses

The SRM inherently has salient poles on both rotor and stator that make its windage losses much bigger than those have equivalent cylindrical rotor (induction machine, etc.) of the same diameter. To solve this problem, the slots on the rotor can be filled by non-magnetic materials (resin, fiber, etc.) to make the rotor equivalent to a cylinder.

After this, the rotor of the SRM can be approximately considered as a long rotating cylinder encased in a stationary hollow cylinder, of which the air friction losses can be calculated by

$$P_{f,air} = c_f \pi \rho_{air} \omega^3 r_r^4 L_{stk} \tag{19}$$

For the designed SRM, the friction coefficient c_f can be obtained by

$$c_f = 0.46 \left[g(g+r_r)/r_r^2 \right]^{0.25} / Re_g^{0.5} \tag{20}$$

The Couette Reynolds number Re_g can be calculated by

$$Re_g = \rho_{air} r_r \omega g / \mu_a \tag{21}$$

In the SRM under study, the sum of the three kinds of losses mentioned above can be considered as the total power loss of the machine:

$$P_{total-SRM} = P_{cu} + P_{fe} + P_{f,air} \tag{22}$$

In this article, the total power loss is calculated over the whole speed range including the motoring and the generating ranges. Fig.5 shows the plot of the total power loss versus speed.
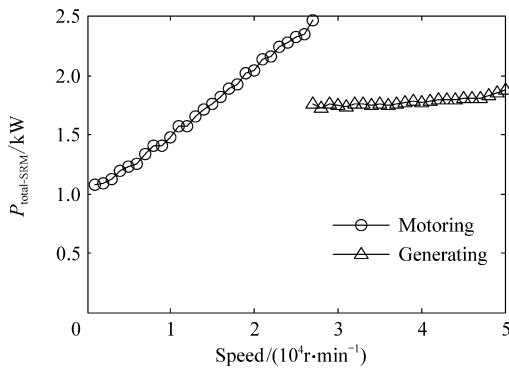
Fig.5   Total power loss of SRM vs operating speed.

4.2. Thermal model of SRM

The thermal model proposed by P. Mellor and D. Turner, et al.[16] has long been adopted as a reference by the researchers working on induction motor thermal problems. J. Faiz, et al.[17] introduced it into thermal analysis of SRM. The Mellor and Turner thermal network is very accurate. However, since several convection heat exchanges are considered in the model and because of the complex geometry and air flows involved, it is difficult to compute all the parameters in Mellor and Turner model. In Ref.[18], a simplified thermal model for variable-speed self-cooling induction motor was proposed, the network has enough accuracy, and what's more, its parameters can be obtained analytically. In this article, a relatively simple thermal model suitable for the thermal analysis of SRM is built based on Ref.[16] and Ref.[18].

Before building the thermal model, many hypotheses should be assumed firstly. In this article, the hypotheses are the same as those in Ref.[18], such as the inner heat sources are uniformly distributed. With the hypotheses, all the thermal resistances can be easily computed based on the thermal network for a single elementary hollow cylinder proposed by Mellor and Turner as shown in Fig.6.
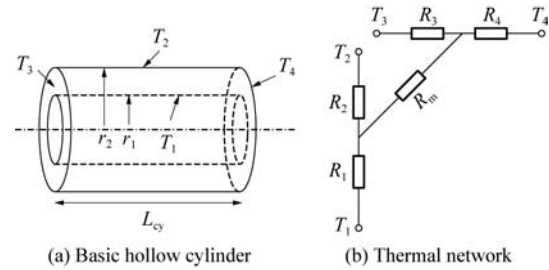
Fig.6   Elementary thermal network proposed by P. Mellor and D. Turner.

In Fig.6, T_1 and T_2 represent the temperature of the inner and outer surfaces, T_3 and T_4 the temperature of the lateral surfaces of the cylinder, r_1 and r_2 the inner and outer radius of the cylinder, L_{cy} is the length of the cylinder, R_1 and R_2 represent the thermal conduction resistance in the radial direction, R_3 and R_4 represent the thermal conduction resistance in the axial direction, R_m takes into account the heat that is not transferred in the previous resistances.

Thermal resistance R_m has to be considered from the theoretical point of view, though always neglected in practice. If the axial thermal flux in a basic cylinder is neglected, the elementary thermal network can be reduced into the following form (see Fig.7).
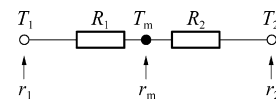

Fig.7   Simplified thermal network for a hollow cylinder.

In Fig.7, T_m is the average temperature corresponding to the average radius r_m. R_1 and R_2 can be computed by the well-known equations of heat transfer in hollow cylinders[19]:

$$R_1 = \frac{1}{2\pi k_{cy} L_{cy}} \ln \frac{r_m}{r_1} \tag{23}$$

$$R_2 = \frac{1}{2\pi k_{cy}L_{cy}}\ln\frac{r_2}{r_m} \tag{24}$$

where $r_m=(r_1+r_2)/2$.

Based on the derivation of the simplified thermal network for a hollow cylinder mentioned above, the thermal model for the designed SRM can be easily built as shown in Fig.8.
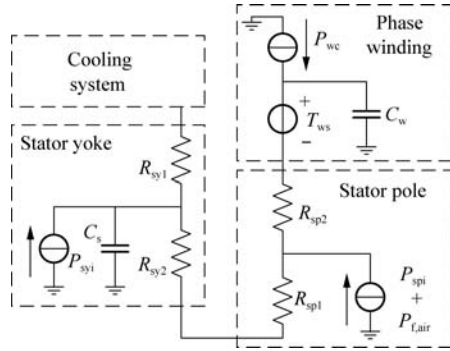

Fig.8   Lumped parameter thermal model of SRM.

For simplicity, the rotor and shaft are not included in Fig.8. This is reasonable for the SRM under consideration, because

1) In the rotor and shaft, only iron losses occur. The total power loss of them are much less than that of the stator.

2) The rotating speed of the rotor is so high in the generating mode that only a small portion of the power losses in the rotor and shaft dissipates through the stator.

In Fig.8, it can be seen that the thermal model of SRM can be mainly divided into four parts. The thermal resistances can be computed based on the dimensions obtained in Section 3 and constant heat transfer coefficients of the material used in the design.

R_{sy1} and R_{sy2} are the outer and inner half part radial conduction resistances of the stator yoke respectively. They can be computed by Eq.(25) and Eq.(26) obtained from Eq.(23) and Eq.(24).

$$R_{sy1} = \frac{1}{2\pi k_{ir}L_{stk}}\ln\frac{r_s}{r_{msy}} \tag{25}$$

$$R_{sy2} = \frac{1}{2\pi k_{ir}L_{stk}}\ln\frac{r_{msy}}{r_s - y_s} \tag{26}$$

where r_{msy} is the average radius of the stator yoke, which can be calculated by

$$r_{msy} = r_s - y_s/2 \tag{27}$$

The definition of the average radius is given in appendix at the end of this article.

R_{sp1} and R_{sp2} are the outer (near the yoke) and inner half part radial conduction resistances of the stator pole respectively, which take into account the thermal

flux from the stator teeth to the stator yoke. This part is considered equivalent to a cylinder, and R_{sp1} and R_{sp2} can be computed through the equations similar to Eq.(25) and Eq.(26) except that the equivalent axial length of the cylinder should be changed from L_{stk} to $f_{r(x)}L_{stk}$, where $f_{r(x)}$ is a reduction factor representing the ratio of the pole iron volume to the total volume of the pole plus slots. For example, the reduction factor of R_{sp1} can be obtained from

$$f_{r(sp1)} = \frac{3d_s t_s}{\pi[(r_s - y_s)^2 - (r_s - y_s - d_s/2)^2]} \tag{28}$$

The voltage source T_{ws} denotes the temperature difference between the phase winding and the stator lamination ranging from 5 K to 10 K according to practical experiences.

The current sources in Fig.8 represent the power losses in SRM, where P_{syi} and P_{spi} are the iron losses in the stator yoke and the stator pole respectively. P_{wc} is the phase winding copper losses.

In order to estimate the transient thermal behavior of SRM, thermal capacitances should be added to the model: C_s and C_w represent the thermal capacity of the stator and winding respectively, which can be computed from

$$C = dC_m V \tag{29}$$

where C is the heat capacity, d the density of the material, C_m the specific heat capacity of the material and V the volume.

The detailed thermal model of the cooling system is not included in Fig.8. It is related to the cooling method adopted which will be discussed just below.

4.3. Design of cooling system

As is clear to all, there are basically three fundamental modes of heat transfer: conduction, convection, and radiation. For low power machine, free convection and radiation with the typical heat transfer coefficient of 10-20 W/(m²·K) are sufficient for cooling. For medium power machine, forced air convection is widely used with the typical heat transfer coefficient of 25-250 W/(m²·K). And for high power machine, forced liquid convection is a good choice with the typical heat transfer coefficient of 50-20 000 W/(m²·K). In this article, the SRS/G system under study is a high power system, and the power density of the SRM is high as well. Based on detailed comparisons among several cooling methods, forced water-cooling is adopted finally.

Figs.9-10 show the cross-sectional view of the machine with water channels (marked by shadow) and a photo of the stator and rotor laminations respectively.
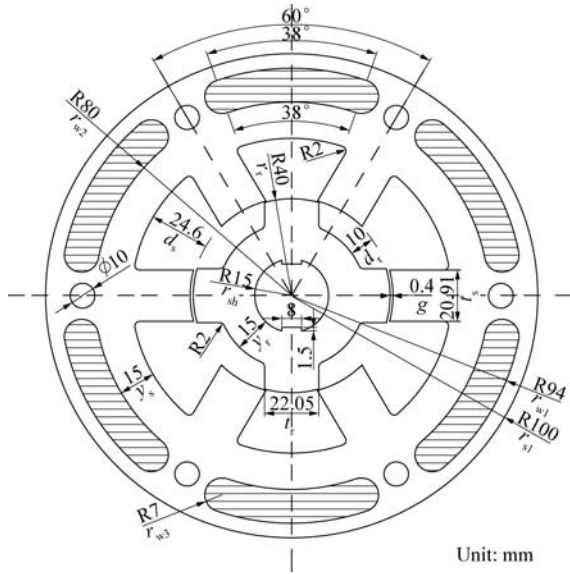
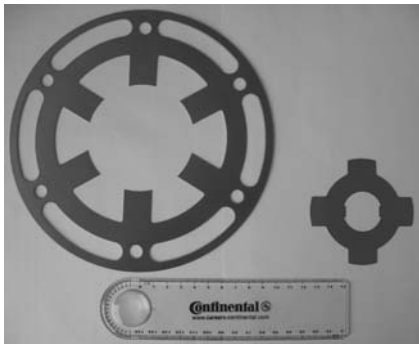Fig.9   Cross-sectional view of machine with water channels.

Fig.10   A photo of stator and rotor laminations.

From Figs.9-10, it can be seen that the water channels are included in the laminations of the stator. This configuration can significantly improve the cooling effects by eliminating the contact thermal resistance between the cooling system and the stator lamination, and what's more, it will only affect the performance of the machine slightly.

4.4. Thermal model of cooling system

Fig.11 shows the thermal model of the cooling system. It comprises surface cooling and water cooling. Surface cooling refers to free air convection and radiation taking place on the outer surface of the machine. Water cooling represents forced convection through the water-cooling system mentioned above.

In Fig.11, T_a and T_w represent the temperature of the ambient and the water respectively. In this article, T_a=313 K (40 °C) and T_w=333 K (60 °C). R_{sc} and R_{wc} denote the thermal resistance of the surface cooling and water cooling respectively. C_c is the thermal capacitance of the whole cooling system which can be obtained by Eq.(29).
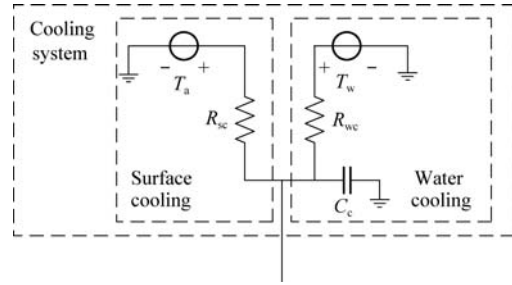
Fig.11   Detailed thermal model of cooling system.

The thermal resistance R_{sc} can be calculated by

$$R_{sc} = \frac{1}{h_{sc}A_{os}} \qquad (30)$$

As mentioned above, the typical heat transfer coefficient of the combination of free air convection and radiation is 10-20 W/(m²·K). In Eq.(30), 10 W/(m²·K) is chosen.

A_{os} can be easily obtained by

$$A_{os} = 2\pi r_{s1}L_{stk} \qquad (31)$$

R_{wc} can be obtained from the equation similar to Eq.(30),

$$R_{wc} = \frac{1}{h_{wc}A_{ws}} \qquad (32)$$

The calculation of h_{wc} is not very easy. It should be done in the following four steps[20].

(1) Calculation of the hydraulic diameter

Because the cross section of the water channels shown in Figs.9-10 is noncircular, the hydraulic diameter D_h should be calculated firstly.

$$D_h = \frac{4A_c}{P} \qquad (33)$$

where A_c and P are cross-section area and passage's wetted perimeter of the water channel, respectively. They can be calculated by

$$A_c = \pi\left[r_{w3}^2 + (r_{w1}^2 - r_{w2}^2)\frac{38°}{360°}\right] \qquad (34)$$

$$P = 2\pi\left[r_{w3} + (r_{w1} - r_{w2})\frac{38°}{360°}\right] \qquad (35)$$

(2) Calculation of the Reynolds number

As a measure to judge if the flow in a forced convection system is laminar or turbulent, the Reynolds number is calculated by

$$Re_{D_h} = \frac{u_{av}D_h}{v} \qquad (36)$$

where u_{av} is the average velocity of the water. In this article, u_{av}=10.4 m/s.

Typically, the Reynolds number for turbulent transition in a noncircular channel is approximately equal to the value of the circular tube of about 2 300. In this article, the Reynolds number obtained from Eq.(36) is equal to 5.287×10⁵. It is far beyond 2 300, so the flow in the designed cooling system must be fully turbulent.

(3) Calculation of the Nusselt number

Because the flow is fully turbulent, the Nusselt number can be got by the Gnielinski's equation,

$$Nu_{D_h} = \frac{\frac{1}{8} f_w (Re_{D_h} - 1\,000) Pr}{1 + 12.7 \sqrt{\frac{1}{8} f_w} (Pr^{2/3} - 1)} \qquad (37)$$

For a smooth tube, the friction factor f_w can be estimated by

$$f_w = \left[0.790 \ln Re_{D_h} - 1.64 \right]^{-2} \qquad (38)$$

The Prandtl number can be directly found in related tables. In this article, the temperature of the water is 333 K, so the Prandtl number is equal to 3.

(4) Calculation of the heat transfer coefficient

The heat transfer coefficient can be determined by

$$h_{wc} = Nu_{D_h} k_w / D_h \qquad (39)$$

A_{ws} in Eq.(32) can be obtained by

$$A_{ws} = 6 P L_{stk} \qquad (40)$$

With the above equations, the thermal resistances of the surface cooling and water cooling can be obtained as follows:

$$\left. \begin{array}{l} R_{sc} = 1.989 \text{ K/W} \\ R_{wc} = 2.926\,7 \times 10^{-4} \text{ K/W} \end{array} \right\} \qquad (41)$$

4.5. Simulation results

Based on the thermal model of the water-cooled SRM built above, the thermal behavior of the machine can be estimated by simulation.

Fig.12 shows the transient temperature curve of the winding at 5.0×10^4 r/min in the generating mode.
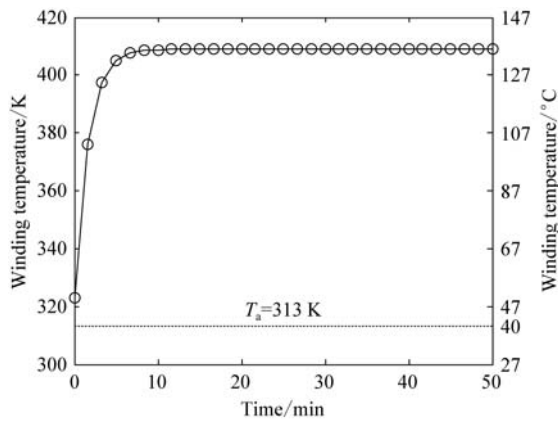
Fig.12　Transient temperature curve of winding at 5.0×10^4 r/min.

From Fig.5, it is discovered that the greatest power losses in SRM occur at 2.7×10^4 r/min in the motoring mode, but it is not the real worst case for thermal analysis. The starting process of engine completes in

only 30 s, whereas the thermal time constant of the machine is very big. It can be seen from Fig.12 that it will take about 8 min for the temperature achieving its steady-state value. Therefore, the thermal behavior of SRM should be considered only in the generating mode and the real worst case for thermal analysis will take place at 5.0×10^4 r/min (Fig.12).

By adopting H-class insulation, the maximum allowable temperature of the winding can reach 453 K (180 °C). In this study, 30 K is set to be the safety margin, so the maximum temperature of the winding should not exceed 423 K (150 °C).

From Fig.12, it can be found that the steady-state temperature of the winding is 415 K (142 °C), which evidences the applicability of the designed forced water-cooling system.

5. Performance Verification and Optimization

The performances of the designed SRM can be evaluated with a PC-based CAD software named PC-SRD developed by the SPEED Laboratory of the University of Glasgow[15].

Fig.13 shows the torque-speed characteristics of the designed SRM obtained by PC-SRD. Unlike Fig.2, the performance in the generating mode shown in Fig.13 is presented in terms of the shaft torque. It can be seen that the designed SRM satisfies the requirements without any further optimization.
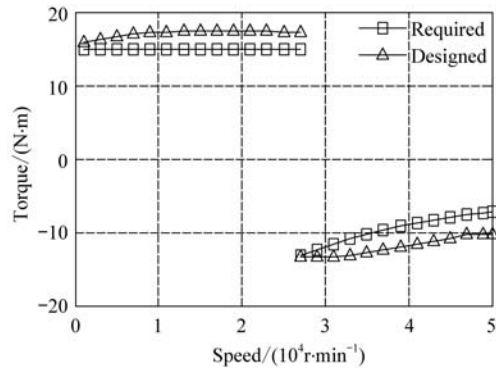
Fig.13　Torque-speed characteristics of designed SRM.

Fig.13 has been acquired on the basis of adopting the simplest control strategy named "all fixed" method, where the turn-on angle θ_{on}, the turn-off angle θ_{off} and the reference current i_{ref} are all fixed.

The "all fixed" method is only used in primary evaluation of the performances of the designed SRM. To get high performances, the exciting angles should be optimized carefully. In this article, the principles of optimization could be introduced as follows.

In the motoring stage, the maximization of the average torque is chosen as an optimization objective to cut down the starting period. Besides, a wider torque-speed envelope and faster transient response will be obtained as well.

In the generating stage, the maximization of the efficiency is chosen as an optimization objective to increase the power density and reduce the energy consumption, thereby lightening the burden of the cooling system.

Taking the motoring mode as an example, Fig.14 shows the optimization results in the motoring mode, including optimal exciting angles and average torque versus operating speed. It can be seen that the average torque increases significantly at both low and high speeds, and a wider torque-speed envelope is obtained.

(a) Optimal exciting angles

(b) Average torque after optimization
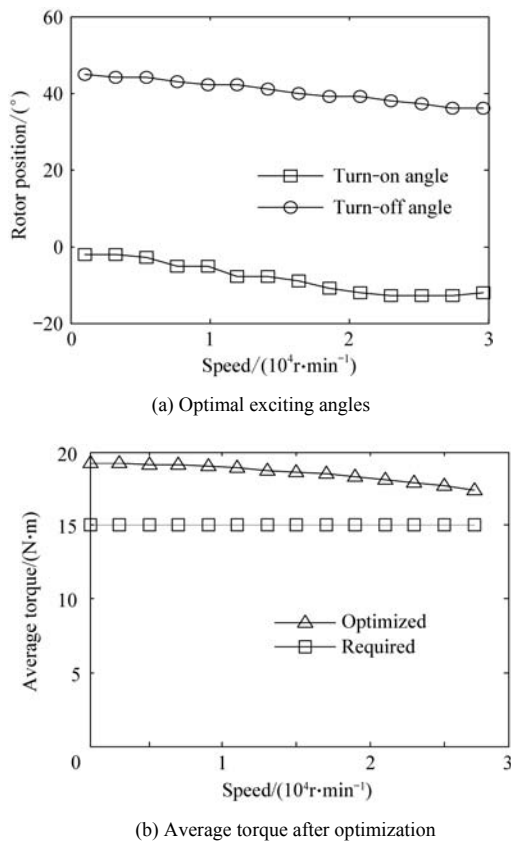
Fig.14   Optimization results in motoring mode.

6. Conclusions

In this article, the fundamental concepts and advantages of the more/all electric aircraft and the combined starter/generator system are briefly addressed. A typical 30 s starting procedure is analyzed in terms of engine speed, temperature and starter torque, and some important performance requirements for CS/G system are obtained. According to these requirements, a high speed SRM is designed.

The design process of the SRM is detailed described from two aspects: electromagnetic design and thermal design. In the electromagnetic design, the dimension of the SRM and the number of phase winding turns per pole are derived in detail. The topology and main technical details of the converter are briefly introduced

as well. In the thermal design, a forced water-cooling system is designed. The thermal model of the SRM, including the designed cooling system, is built. The transient temperature curve of the winding in the real worst-case proves the applicability of the designed cooling system.

The performances of the designed SRM are verified by the torque-speed characteristics obtained by PC-SRD. To get high performances, the exciting angles are optimized in both operating modes separately and the optimized performances in the motoring mode are presented as an example.

At present, a prototype of the motor is being constructed and its experimental results will be available by the end of 2009.

Acknowledgements

References

[1]   Schaefer U, Vollmer U. An at all operating points highly efficient PMSM for HEV. EVS-23: Sustainability—The Future of Transportation. 2007; 235-240.

[2]   Quigley R E J. More electric aircraft. Eighth Annual Applied Power Electronics Conference and Exposition. 1993; 906-911.

[3]   Jones R I. The more electric aircraft: the past and the future. IEE Colloquium on Electrical Machines and Systems for the More Electric Aircraft. 1999; 1-4.

[4]   Cronin M J J. The all-electric aircraft. IEE Review 1990; 36(3): 309-311.

[5]   Pearson W. The more electric/all electric aircraft—a military fast jet perspective. IEE Colloquium on All Electric Aircraft. 1998; 1-7.

[6]   Malik E E, Kankam M D. Potential starter/generator technologies for future aerospace application. IEEE Aerospace and Electronic Systems Magazine 1996; 11(10): 17-24.

[7]   Weimer J A. The role of electric machines and drives in the more electric aircraft. IEEE International Electric Machines and Drives Conference. 2003; 11-15.

[8]   Ferreira C A, Jones S R, Heglund W S, et al. Detailed design of a 30-kW switched reluctance starter/generator system for a gas turbine engine application. IEEE Transactions on Industry Applications 1995; 31(3): 553-561.

[9]   Schofield N, Long S. Generator operation of a switched reluctance starter/generator at extended speeds. IEEE Conference on Vehicle Power and Propulsion. 2005; 453-460.

[10]   Radun A V, Ferreira C A, Richter E. Two-channel switched reluctance starter/generator results. IEEE Transactions on Industry Applications 1998; 34(5): 1026-1033.

[11]   Huenecke K. Jet engines: fundamentals of theory, design and operation. Ramsbury: Airlife Publishing Ltd., 1997.

[12]   Miller T J E. Switched reluctance motors and their control. Oxford: Clarendon Press, 1993.

[13] Krishnan R, Arumugam R, Lindsay J F. Design procedure for switched-reluctance motors. IEEE Transactions on Industry Applications 1988; 24(3): 456-461.

[14] Saari J. Thermal analysis of high-speed induction machines. PhD thesis, Helsinki University of Technology, 1998.

[15] Miller T J E. SPEED's PC-SRD Version8.7 user's manual. Glasgow: SPEED Laboratory, University of Glasgow, 2007.

[16] Mellor P, Roberts D, Turner D. Lumped parameter thermal model for electrical machines of TEFC design. IEE Proceedings B: Electric Power Applications 1991; 138(5): 205-218.

[17] Faiz J, Iranpour R. Thermal model for a switched reluctance motor of TEFC design during steady state and transient operation. Electric Machines and Power System 1998; 26(1): 77-91.

[18] Boglietti A, Cavagnino A, Lazzari M, et al. A simplified thermal model for variable-speed self-cooled industry induction motor. IEEE Transactions on Industry Applications 2003; 39(4): 945-952.

[19] Chapman A J. Fundamentals of heat transfer. London: Collier Macmillan Publishers, 1987.

[20] Lienhard J H IV, Lienhard V J H. A heat transfer textbook. Cambridge: Phlogiston Press, 2003.

Biography:

Song Shoujun   Born in 1981, he received B.S. and M.S. degrees from Northwestern Polytechnical University in 2003 and 2006 respectively, and then became a Ph.D. candidate there. He is currently studying at the School of Electrical Engineering and Computer Sciences, Technical University of Berlin, Berlin, Germany, sponsored by China Scholarship Council. His research interests are in electrical machines and drives, especially in design and control optimization.
E-mail: songshoujun@hotmail.com

Appendix A: Definition of the Average Radius

To describe clearly, Fig.A1 shows the definition of the average radius of the yoke and the pole with both the stator and rotor illustrated.
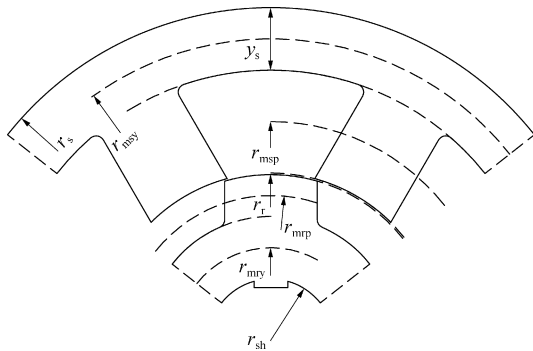

Fig.A1   Definition of average radius of yoke and poles.

In Fig.A1, r_{msy} and r_{msp} represent the average radius of the stator yoke and poles while r_{mry} and r_{mrp} those of the rotor yoke and poles.

Appendix B: Main Physical Quantities Used in Thermal Analysis

As there are many physical quantities involved in the thermal analysis in this article, the way to determine their values should be explained in the following.

Many physical quantities used in this article are related to the temperature. For instance, the relationship between the temperature and the dynamic viscosity of the air μ_a used in Eq.(21) can be expressed as

$$\mu_a = 310 \times 10^{-8} + 5.128 \times 10^{-8} T_{air} \qquad (B1)$$

where T_{air} is the air temperature, K. In this article, T_{air} is equal to the ambient temperature.

The values of the physical quantities can also be easily found in corresponding tables according to the type of material and the temperature.

Sometimes the value cannot be found directly from the table because the relevant working temperature is not included there. In this case, the value can be easily calculated by linear interpolation. Here take the thermal conductivity of water as an example. First, we can find 0.639 6 W/(m·K) at 320 K and 0.660 5 W/(m·K) at 340 K in the related table. Then, the unknown value at the temperature of 333 K can be calculated from

$$k_w = \frac{333 - 320}{340 - 320} \times (0.660\ 5 - 0.639\ 6) + 0.639\ 6 = 0.653\ 2 \qquad (B2)$$

Table B1 lists the temperature and the values of the physical quantities used in this article.

Table B1   Values of physical quantities

Symbol	Value
T_a/K	313
T_w/K	333
ρ_{air}/(kg·m^{-3})	1.112
μ_a/(kg·(s·m)$^{-1}$)	1.915×10^{-5}
k_{ir}/(W·(m·K)$^{-1}$)	58
v/(m^2·s^{-1})	4.748×10^{-7}
k_w/(W·(m·K)$^{-1}$)	0.653 2